International Journal of Mass Spectrometry 273 (2008) 24–30

Contents lists available at ScienceDirect

International Journal of Mass Spectrometry

journal homepage: www.elsevier.com/locate/ijms

Infrared multiple-photon photodissociation of gas-phase group II metal-nitrate anions

Jos Oomens[a], Linda Myers[b,1], Ryan Dain[b], Chris Leavitt[b], Vy Pham[b], Garold Gresham[c], Gary Groenewold[c], Michael Van Stipdonk[b,*]

[a] FOM Institute for Plasma Physics "Rijnhuisen", Edisonbaan 14, NL-3439 MN Nieuwegein, The Netherlands
[b] Department of Chemistry, Wichita State University, 1845 Fairmount, Wichita, Kansas 67260-0051, USA
[c] Idaho National Laboratory, Idaho Falls, ID 83415-2208, USA

ARTICLE INFO

Article history:
Received 12 December 2007
Received in revised form 10 February 2008
Accepted 13 February 2008
Available online 29 February 2008

Keywords:
IRMPD
Photodissociation
Metal ion
Electrospray ionization
Density functional theory

ABSTRACT

Infrared spectra of gas-phase metal-nitrate anions $M(NO_3)_3^-$, where M = Mg^{2+}, Ca^{2+}, Sr^{2+} and Ba^{2+}, were recorded by infrared multiple-photon dissociation (IRMPD) spectroscopy. Photodissociation of each of the precursors produces NO_3^- through the elimination of a neutral $M(NO_3)_2$ unit. An absorption pattern characteristic of metal nitrates is observed in the IRMPD spectra, including the symmetric and antisymmetric NO_3 stretches. The latter is split into high-and low-frequency components as a result of perturbation of the nitrate symmetry by complexation to the metal ion, and the magnitude of the splitting decreases following the trend $Mg^{2+} > Ca^{2+} > Sr^{2+} \cong Ba^{2+}$. The experimental spectra are in good general agreement with those obtained from density functional theory (DFT) calculations.

© 2008 Elsevier B.V. All rights reserved.

1. Introduction

Metal nitrate and nitric acid species have been a focus of vibrational spectroscopic studies, primarily because the vibrations of the nitrate anion can function as a sensitive probe of chemical environment. The dominant feature in the infrared spectrum of alkali metal nitrates is the antisymmetric (ν_3) NO_3 stretch at approximately 1360–1400 cm^{-1}. However, matrix isolation spectroscopy (MIS) experiments have shown that for discrete metal nitrate ion pairs the metal distorts the D_{3h} symmetry of the anion, splitting the degenerate ν_3(e) (NO_3^- antisymmetric stretching) mode into the ν_{3a} and ν_{3b} components [1,2]. Within a limited number of systems, the magnitude of the splitting ($\Delta\nu_3$) has been shown to be proportional to the metal binding strength. For example, $\Delta\nu_3$ values of 260 and 171 cm^{-1} were measured for $LiNO_3$ and KNO_3, respectively [1]. For isolated ammonium and hydronium nitrate species the $\Delta\nu_3$ values were ~170 and 150 cm^{-1}, respectively [2].

MIS studies of nitric acid have also revealed the effect of disruption of the nitrate anion symmetry. For isolated HNO_3, an NO_2 antisymmetric stretch near 1700 cm^{-1} was observed, along with NOH bending and symmetric NO_2 modes at 1340 and 1320 cm^{-1}, respectively [3]. In addition, the spectrum of HNO_3 was later found to depend on the extent of hydration. Addition of two H_2O molecules generates a nitric acid dihydrate, giving IR spectra similar to those of nitrate, with an antisymmetric nitrate doublet at 1440 and 1270 cm^{-1}, and the activated symmetric stretching mode at 1040–1029 cm^{-1} [4–6]. These results were interpreted in terms of the highly asymmetric NO_3 stretch in the dihydrate complex, distinct from absorptions attributed to the monohydrate and trihydrate, which showed only a single nitrate antisymmetric stretch mode at about 1390 cm^{-1} [7,8].

Complications arising from interactions with the local environment, such as with water molecules in solution and to a lesser extent the matrix in MIS, can be avoided when the complexes are studied in complete isolation in the gas-phase. The combination of ion-trapping mass spectrometers and photodissociation using IR free electron lasers has provided unprecedented access to the vibrational spectra of discrete, gas-phase metal ion complexes [9–18]. Acquisition of conventional linear absorption spectra is generally not possible because of the extremely low ion densities in an ion trap mass spectrometer. However, using an action spectroscopy approach, photon absorption can be monitored by measuring fragmentation yields from wavelength-selected infrared multiple-photon photodissociation (IRMPD) [19–21].

Our group recently applied wavelength-selective IRMPD to generate the first vibrational spectra of gas-phase metal-nitrate

* Corresponding author. Tel.: +1 316 978 7381; fax: +1 316 978 3431.
E-mail address: mike.vanstipdonk@wichita.edu (M. Van Stipdonk).
[1] Present address: Department of Chemistry, Benedictine College, 1020 North 2nd Street, Atchison, KS 66002, USA.

1387-3806/$ – see front matter © 2008 Elsevier B.V. All rights reserved.
doi:10.1016/j.ijms.2008.02.013

anions, focusing on $[UO_2(NO_3)_3]^-$ and $[Eu(NO_3)_4]^-$ [22]. The experiments were performed using the Free Electron Laser for Infrared Experiments (FELIX) at the FOM Institute for Plasma Physics in Nieuwegein, The Netherlands, which delivers a high intensity beam of photons at wavelengths across the mid-IR range to a dedicated high-resolution mass spectrometer. The IRMPD spectra of both $[UO_2(NO_3)_3]^-$ and $[Eu(NO_3)_4]^-$ are dominated by the nitrate antisymmetric ν_3 stretch. As in matrix isolated spectra of metal-nitrate species, the ν_3 stretch is split into high- and low-frequency components. The higher frequency component, measured at about 1537 and 1542 cm^{-1} for the UO_2^{2+} and Eu^{3+} complexes, respectively, corresponds to the terminal, non-coordinating N=O group, while the lower frequency absorption (at 1272 and 1264 cm^{-1} for UO_2^{2+} and Eu^{3+}, respectively) is attributed to the antisymmetric O—N—O stretch that involves the O atoms that coordinate the metal center. The $\Delta\nu_3$ values are thus 264 and 273 cm^{-1} for the UO_2^{2+} and Eu^{3+} species, respectively, comparable to the value measured previously for $LiNO_3$ using MI spectroscopy [1].

In the experiments presented here, the IRMPD approach was used to generate vibrational spectra of anionic complexes with general formula $[M(NO_3)_3]^-$, where M = Mg^{2+}, Ca^{2+}, Sr^{2+} and Ba^{2+}. Following trends down the group II species allows a systematic investigation of the influence of the polarizing power of the cation on the diagnostic splitting of ν_3. Density functional theory (DFT) calculations were performed to determine the lowest-energy structures for each of the anions, to confirm peak assignments in the infrared spectrum and to further assess structural trends of the group II metal-nitrate complexes.

2. Experimental

2.1. Generation of metal-nitrate anions by ESI

Metal (Mg^{2+}, Ca^{2+}, Sr^{2+} and Ba^{2+}) nitrate salts were purchased from Sigma–Aldrich (Zwidrecht, The Netherlands) and used as received. For health and safety reasons, the Be^{2+} salt was not included in these experiments. Spray solutions for ESI were prepared by dissolving the metal-nitrate salt in a 1:1 mixture of deionized water and HPLC-grade methanol to generate concentrations of ~1 mM.

The anionic metal-nitrate species were generated in a home-built Fourier transform ion cyclotron resonance (FT-ICR) mass spectrometer at the FOM Institute for Plasma Physics in Nieuwegein, The Netherlands. The mass spectrometer is equipped with a Z-spray electrospray ionization source (Micromass, Manchester, UK) that produces ions at atmospheric pressure in a spray plume orthogonal to a sampling cone. Ions are accumulated in the hexapole trap of the ESI source prior to being injected into the ICR cell via a quadrupole deflector and a 1-m long octapole ion guide. Rapid switching of the DC bias of the octapole during the ion transfer allows for capture of the ions in the ICR cell without the use of a gas pulse, thus avoiding collisional heating of the ions [23]. Abundant ions corresponding to $M(NO_3)_3^-$ were detected in the mass spectrum, and isolated for IRMPD study using a stored waveform inverse Fourier transform (SWIFT) pulse [24] which ejects all species except those having the desired mass.

2.2. Infrared multiple-photon dissociation (IRMPD)

Infrared spectra are collected by monitoring the efficiency of IRMPD as a function of laser wavelength. After mass-selective isolation, the precursor ions are irradiated using ten FELIX macropulses (40 mJ per macropulse, 5 μs pulse duration, bandwidth 0.2–0.5% of central λ). IRMPD occurs through non-coherent absorption of tens to hundreds of IR photons, when the laser frequency matches a vibrational mode of the gas-phase ion. The energy is distributed over all vibrational modes by intramolecular vibrational redistribution (IVR). The IVR process allows the energy of each photon to be "relaxed" prior to the absorption of the next photon, and thus allows promotion of the ion's internal energy to the dissociation threshold [25]. Prior studies have shown that the infrared spectra obtained using IRMPD are comparable to those obtained using linear absorption techniques [4,26].

To produce infrared spectra, the free electron laser was scanned in 0.02–0.04 μm increments between 6 and 12.5 μm, with measurement of product ions and un-dissociated precursor ions using the excite/detect sequence of the FT-ICR-MS [27] after irradiation with FELIX. The IRMPD yield is normalized to the total ion yield, and corrected for variations in FELIX power over the spectral range.

2.3. Molecular structure and frequency calculations

The Gaussian 03 group of programs [28] was used for density functional theory calculations in support of the IRMPD investigation. Full geometry optimizations and frequency calculations were performed for the bare nitrate anion and for complexes with general formula $[M(NO_3)_3]^-$, $[M(NO_2)_2]$ and $[M(NO_3)]^+$. The geometry optimization and frequency calculations for $[M(NO_3)_3]^-$ were used for direct comparison to IRMPD spectra. The calculations for $[M(NO_3)_2]$ and $[M(NO_3)]^+$ were performed to probe the influence of the number of nitrate ligands within a complex on the positions of symmetric and antisymmetric NO_3 stretches, and the magnitude of the splitting of the former due to interactions with the metal ion. The B3LYP functional [29,30] was used for all calculations. Our goal was not to assess the absolute accuracy of DFT methods for predicting vibrational frequencies for the metal-nitrate anions, but rather to use the DFT-generated frequencies to confirm assignment of bands in the IRMPD spectrum. Therefore, calculations using other functionals or computational models were not attempted, nor were calculations of precursor ion dissociation energies.

For the Mg^{2+} and Ca^{2+} species geometry optimizations were initiated using the B3LYP functional and the 3–21 g* basis set. Initial geometry optimizations for the Sr and Ba species were instead performed using a gen basis set approach in which a Stuttgart–Dresden-type (SDD) pseudopotential [31–34] and associated basis set was used for the metal ion (MWB28 and MWB46 for Sr and Ba, respectively) and the 3–21 g* basis set for N and O. The preliminary geometries for each species were then re-optimized using the B3LYP functional and larger basis sets. For the Mg^{2+} and Ca^{2+} species, the 6-311 + g(2d,p) basis set was used on the metal ion and the 6-311 + g(d,p) basis set was applied to N and O. For re-optimization of the Sr^{2+} and Ba^{2+} species, the SDD pseudopotential and basis set was used for the metal atoms, and the 6-311 + g(d,p) basis set was applied to N and O. Frequency calculations were then performed using the same functional and basis sets. For comparison to the experimentally derived spectra, the frequencies generated by DFT are scaled by a factor of 0.98 for inclusion into Fig. 3. As discussed below, the B3LYP functional and the basis sets employed provide good general agreement with the experimental IRMPD spectra.

To probe the relationship between relative complex ion energy, inter-ligand distances and nitrate tilt angle (*vide infra*), a series of single-point calculations are carried out using the B3LYP functional, the gen 6-311 + g(2d,p)/6-311 + g(d,p) basis set combination for $[Mg(NO_3)_3]^-$ and the MWB46/6-311 + g(d,p) combination for $[Ba(NO_3)_3]^-$. The tilt angle, discussed in a later section, is the angle of the nitrate ligands measured relative to the plane defined by the metal cation and the 3 N atoms within the complex (Fig. 1). For measurements of inter-ligand distances, O_1—O_1 refers to the distance between O atoms of adjacent ligands when both occupy the same side of the reference plane used to measure the tilt-angle.

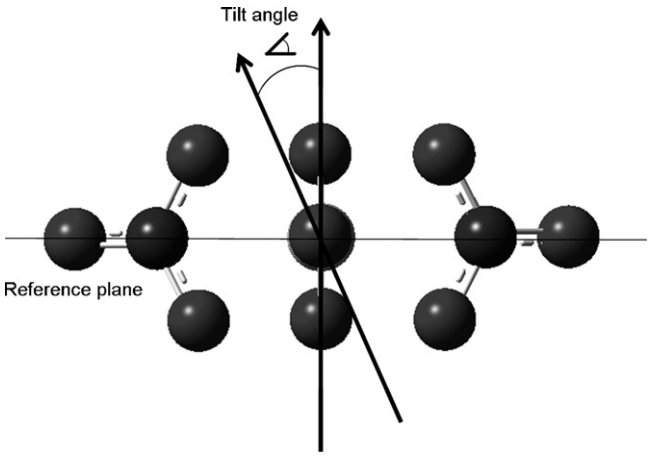

Fig. 1. General $[M(NO_3)_3]^-$ structure with vertical orientation of the nitrate ligands. The tilt angle for the nitrate ligands is measured relative to the horizontal plane defined by the metal cation and the 3 N atoms within the complex. A tilt angle of 90° (as shown here) corresponds to vertically oriented nitrate ligands. The metal atom M is positioned directly behind the O atom in the figure.

Table 1
Bond lengths for lowest energy conformations of the $[M(NO_3)_3]^-$ as determined using DFT

	N=O[a]	N—O	M—O	O_1—O_1
NO_3^-	1.260			
$[Mg(NO_3)]^+$	1.214	1.282	2.120	3.270
$[Ca(NO_3)]^+$	1.217	1.280	2.409	3.783
$[Sr(NO_3)]^+$	1.218	1.279	2.569	4.054
$[Ba(NO_3)^+$	1.221	1.278	2.743	4.361

[a] For NO_3^-, each N—O bond has partial double bond character.

The O_1—O_2 distance corresponds to the distance between O atoms of adjacent ligands that lie on opposite sides of the reference plane. For the single-point calculations, the complexes were initially constructed using the optimized geometry of the nitrate anion (using B3LYP/6-311 + g(d,p)). The nitrate ligands were oriented vertically (90°) and the metal–N and metal–O distances were set at the values taken from the fully optimized structures of either $[Mg(NO_3)_3]^-$ or $[Ba(NO_3)_3]^-$. The single-point calculations were performed by holding the metal–nitrate N atom distance constant and altering the tilt angle from 90° (fully vertical nitrate ligands) to 35°. Tilt angles less than 35° were not considered because the energies of the complexes were increasing dramatically as the angle approached this value (see below).

3. Results and discussion

3.1. Density functional theory calculations for $[M(NO_3)_3]^-$

Optimized structures for $[Mg(NO_3)_3]^-$, $[Ca(NO_3)_3]^-$, $[Sr(NO_3)_3]^-$ and $[Ba(NO_3)_3]^-$ are shown in Fig. 2. For NO_3^- and each $[M(NO_3)_3]^-$ ion, bond lengths and angles from the DFT calculations are provided in Tables 1 and 2, respectively. In each

Table 2
Bond angles for lowest energy conformations of the $[M(NO_3)_3]^-$ as determined using DFT

	O—N—O	O—N=O
NO_3^-		120.0
$[Mg(NO_3)_3]^-$	114.7	122.6
$[Ca(NO_3)_3]^-$	116.1	122.0
$[Sr(NO_3)_3]^-$	116.5	121.7
$[Ba(NO_3)_3]^-$	116.8	121.6

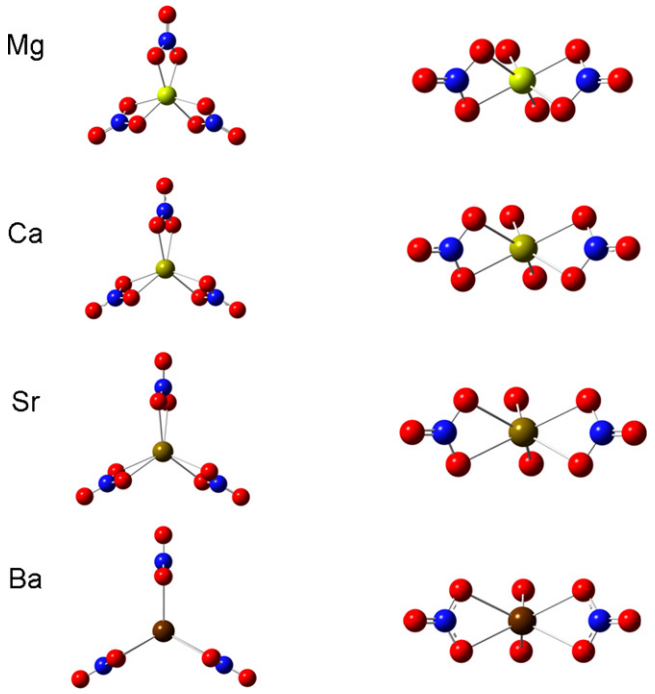

Fig. 2. Lowest energy conformations predicted for the $[M(NO_3)_3]^-$ species where M = Mg^{2+}, Ca^{2+}, Sr^{2+} and Ba^{2+}. Structures were obtained using the B3LYP functional; 6-311 + g(2d,p) basis set on Be^{2+}, Mg^{2+} and Ca^{2+}, MWB26 on Sr^{2+}, MWB48 on Ba^{2+} and 6-311 + g(d,p) basis set on N and O. The left column shows the respective ions as viewed perpendicular to the plane containing the nitrate N atoms and the cation. The right column shows the ions when viewed along the same plane.

$[M(NO_3)_3]^-$ ion, the nitrate ligands are bound to the respective metal ions in a bidentate fashion. Geometry optimizations starting from monodentate nitrate coordination collapsed to the bidentate coordination mode shown in Fig. 2. For $[Mg(NO_3)_3]^-$, the three N atoms and Mg are arranged in trigonal planar geometry. The three NO_3^- ligands are neither coplanar, nor are they normal to the plane. Instead, the ligands are significantly tilted and the complex adopts a 'propeller' conformation. Comparing the structures of the trinitrato Ca^{2+}, Sr^{2+}, and Ba^{2+} complexes, the nitrate anions adopt orientations that become progressively more normal to the metal-nitrogen plane. Relative to the reference plane defined by the metal ion and the three N atoms of the nitrate ligands, the tilt angles in optimized structures are 63.0°, 69.3°, 76.9° and 87.1° for the Mg^{2+}, Ca^{2+}, Sr^{2+} and Ba^{2+} species, respectively.

The pronounced propeller conformation for the Mg and Ca complexes presumably arises as the result of repulsive inter-ligand interaction: repulsion by the O atoms of adjacent nitrate ligands is minimized by tilting. To probe the effect of the tilt angle on the energy of the complex, and for changes in inter-ligand O—O distances, a series of single-point calculations were carried out for the $[Mg(NO_3)_3]^-$ and $[Ba(NO_3)_3]^-$ species. The results derived from the single-point calculations are shown in Figs. 3 and 4 for $[Mg(NO_3)_3]^-$ and $[Ba(NO_3)_3]^-$, respectively. In Figs. 3a and 4a, the O_1—O_1 and O_1—O_2 distances for the respective complexes are shown for tilt angles of the nitrate ligands ranging from 90° (fully vertical) to 35°. For Mg and Ba nitrate complexes, the O_1—O_2 distance (Fig. 1), is larger than the O_1—O_1 distance by 0.663 and 0.507 Å, respectively. With increasing tilt angle, the O_1—O_1 distances increase while the O_1—O_2 distances decrease. For the $[Mg(NO_3)_3]^-$ species, the O_1—O_1 and O_1—O_2 distances are comparable between 60° and 65°, while for $[Ba(NO_3)_3]^-$ the distances are comparable between 65° and 70°. Figs. 3b and 4b show the changes in electronic energy for $[Mg(NO_3)_3]^-$ and $[Ba(NO_3)_3]^-$, respectively, with increasing tilt

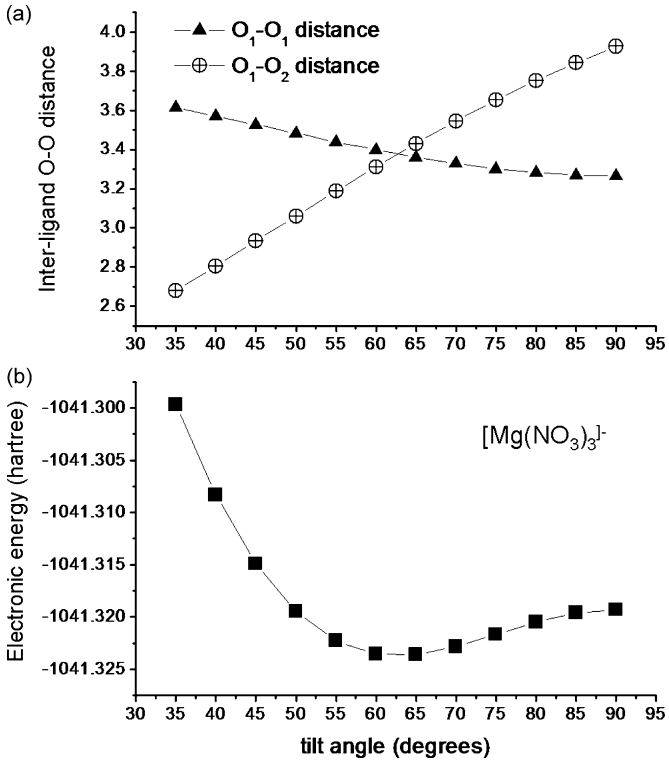

Fig. 3. Influence of nitrate ligand tilt angle on (a) the O_1—O_1 and O_1—O_2 distances and (b) overall complex electronic energy for $[Mg(NO_3)_3]^-$ as determined using single-point calculations (B3LYP/6-311 + g(2d,p)/6-311 + g(d,p)).

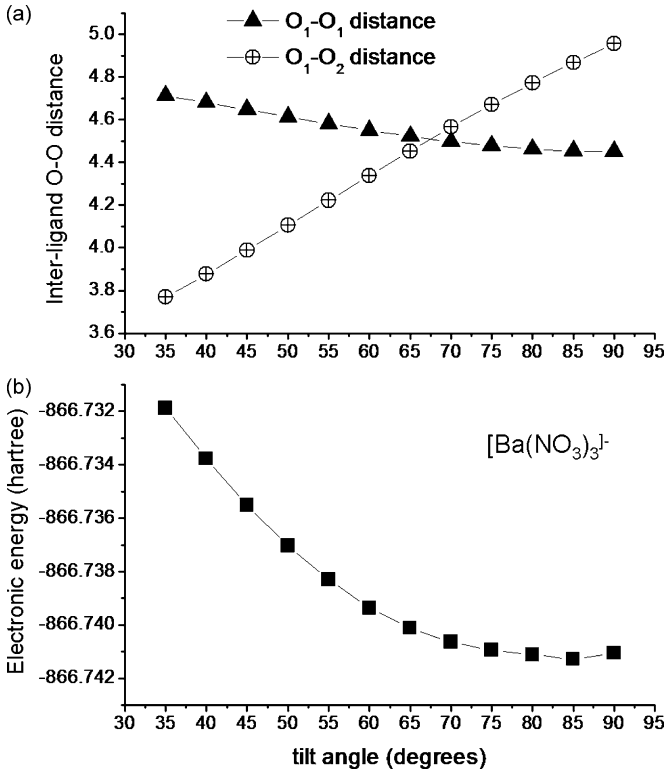

Fig. 4. Influence of nitrate ligand tilt angle on (a) the O_1—O_1 and O_1—O_2 distances and (b) overall complex electronic energy for $[Ba(NO_3)_3]^-$ as determined using single-point calculations (B3LYP/6-311 + g(2d,p)/6-311 + g(d,p)).

angle. For $[Mg(NO_3)_3]^-$, the energy of the complex decreases to a minimum at approximately 65°, and then increases with further increase of the tilt angle. The energy minimum derived from the single-point energy calculations corresponds well with the tilt angle of ~63° observed for the optimized structure of $[Mg(NO_3)_3]^-$ as shown in Fig. 2. Based on a comparison of the data in Fig. 3a and b, it appears that the increasing O_1—O_1 distances with increasing tilt angle lowers the complex energy (presumably by minimizing repulsion) until the minimum at ca. 60–65°. Beyond this tilt angle, the sharper decrease in O_1—O_2 distance, and thus greater potential repulsion by the O atoms, significantly influences the complex energy.

As shown in Fig. 4b for $[Ba(NO_3)_3]^-$, the complex energy decreases slightly to a minimum at 85°, increases slightly for tilt angles of 85–70°, and then undergoes a more pronounced increase for tilt angles less than 65°. The minimum observed in Fig. 4b is close to the ~87° tilt angle predicted for the optimized structure described above. In general, the effect on complex energy with changes in tilt angle from 90° to 70° is less pronounced for the Ba complex than for the Mg analog, which suggests that there is less energetic driving force for the nitrate ligands to adopt tilted configurations to minimize repulsive interactions within the complexes that contain the larger cations. The effect of the tilt angle on relative energies and inter-ligand O—O atom distances for the Ca- and Sr-containing complexes is expected to be intermediate between values calculated for complexes of Mg and Ba, which is supported by the tilted nitrate ligands predicted for the minimized structures shown in Fig. 2.

The DFT calculations, with the functional and basis sets used here, predict equivalent N—O bond lengths of 1.260 Å for the bare nitrate anion. Bonding to the metal ion within the $[M(NO_3)_3]^-$ anion distorts the symmetry of the anion, creating non-coordinating N═O and metal-coordinating N—O groups. Compared to bare nitrate, the N═O bond length in the $[Mg(NO_3)_3]^-$anion is substantially decreased to 1.214 Å (Table 1). The N═O bond length increases following the trend $Mg^{2+} < Ca^{2+} < Sr^{2+} < Ba^{2+}$, suggesting that the bond systematically weakens with increasing cation radius and decreasing polarizing power. The N—O bond length (coordinating O atoms) is increased (to 1.282 Å) in $[Mg(NO_3)_3]^-$ compared to the N—O bond lengths in the bare nitrate anion. Thus, as the cation polarizing power increases (decreasing metal ionic radius), so does the N—O bond length, while the N═O bond length decreases.

The O—N—O and O—N═O bond angles of the $[M(NO_3)_3]^-$ species were also found to depend on the ionic radius of the metal (Table 2). The O—N—O angle connects the two O atoms that coordinate the metal ion, while the O—N═O angle involves the terminal, non-coordinating O atom. Thus, as the cation polarizing power increases, the O—N—O angle decreases and the O—N═O angle must increases. For example, the O—N—O angle decreases from 116.8 for the Ba^{2+} complex to 114.7 for the Mg^{2+} version, while the O—N═O angle increases from 121.6 for the Ba^{2+} complex to 122.6 for the Mg^{2+} version.

3.2. IRMPD of $[M(NO_3)_3]^-$

Fig. 5 shows mass spectra generated during an IRMPD run for $Mg(NO_3)_3^-$ and are representative of those collected for each of the $M(NO_3)_3^-$ precursor ions. The mass spectrum of $[Mg(NO_3)_3]^-$ isolated using a SWIFT pulse and irradiated at 1600 cm^{-1} is shown in Fig. 5a. At this wavelength, FELIX was "off-resonance" with absorptions of the complex and no photodissociation of $Mg(NO_3)_3^-$ is observed. The mass spectrum shown in Fig. 5b was obtained when $Mg(NO_3)_3^-$ was irradiated at approximately 1500 cm^{-1}, near the resonance of the high-frequency N═O antisymmetric stretch of the nitrate ligands (see below). IR induced photodissociation results in the elimination of a neutral $Mg(NO_3)_2$ unit to leave NO_3^-. Similar dissociation pathways are observed for each of the group II nitrate anions. To generate IRMPD spectra, the NO_3^- yield from each of the

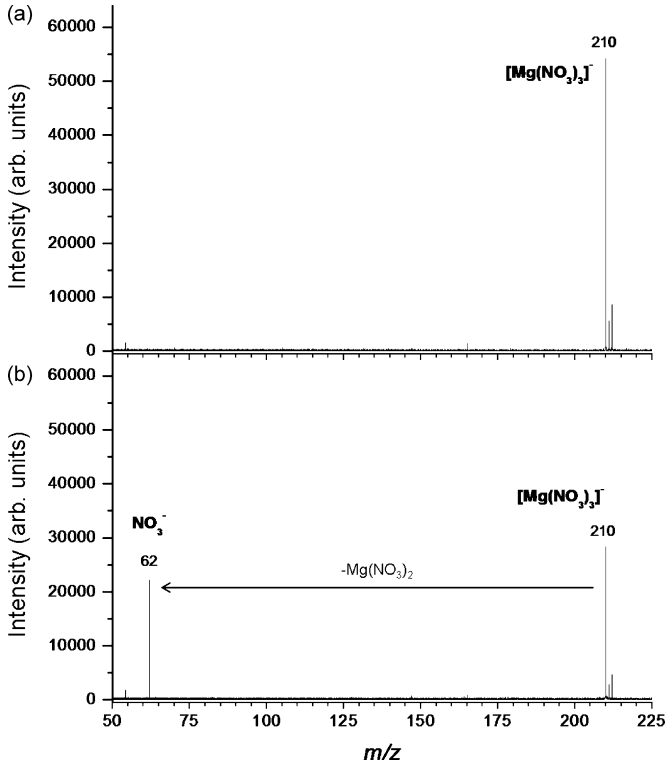

Fig. 5. Mass spectra generated from an experiment involving IRMPD of $[Mg(NO_3)_3]^-$: (a) spectrum produced following isolation of $[Mg(NO_3)_3]^-$ and irradiation "off-resonance" with light at ca. 1600 cm^{-1}, (b) spectrum following isolation of the same species with irradiation "on-resonance" at ca. 1500 cm^{-1}. Absorption of IR photons induced photodissociation pathway that involves elimination of $Mg(NO_3)_2$.

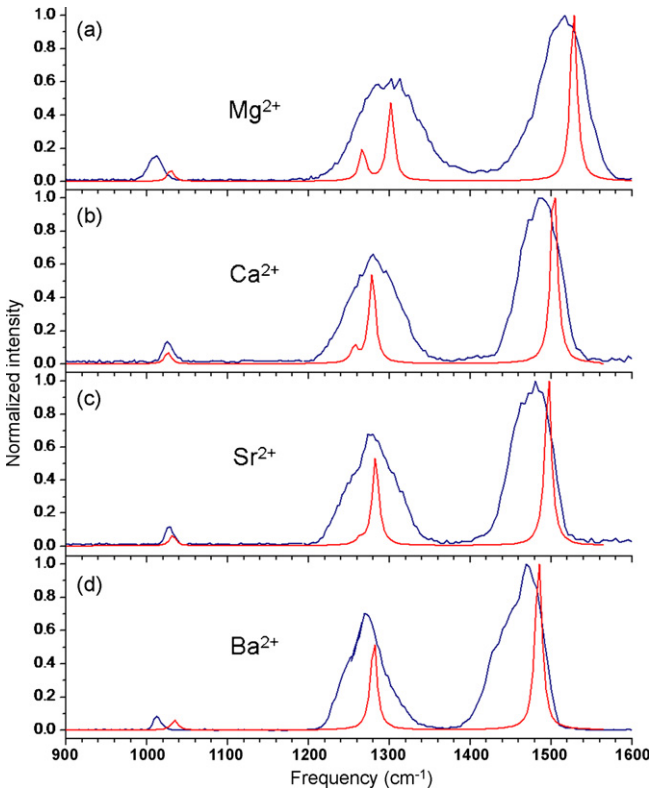

Fig. 6. IRMPD results for $[M(NO_3)_3]^-$: (a) $[Mg(NO_3)_3]^-$, (b) $[Ca(NO_3)_3]^-$, (c) $[Sr(NO_3)_3]^-$, and (d) $[Ba(NO_3)_3]^-$. In each spectrum, the blue (dark) trace corresponds to the experimental IRMPD spectrum while the red (lighter) trace represents the spectrum predicted by DFT.

Table 3
Best estimates of the centroids of peaks in the experimental IRMPD spectra of $[M(NO_3)_3]^-$

	N=O	O—N—O (ν_3)	$\Delta\nu_3$	Sym. NO_3 (ν_1)
$[Mg(NO_3)_3]^-$	1517	1298	219	1011
$[Ca(NO_3)_3]^-$	1487	1279	208	1009
$[Sr(NO_3)_3]^-$	1476	1276	200	1010
$[Ba(NO_3)_3]^-$	1469	1271	198	1009

$M(NO_3)_3^-$ precursor ions was monitored as FELIX is scanned from approximately 1800 to 900 cm^{-1}.

Fig. 6 shows the IRMPD spectra of $Mg(NO_3)_3^-$, $Ca(NO_3)_3^-$, $Sr(NO_3)_3^-$ and $Ba(NO_3)_3^-$. The experimental spectra are compared to theoretical spectra derived from DFT calculations (B3LYP/6-311 + g(2d,p)/6-311 + g(d,p) or B3LYP/SDD/6-311 + g(d,p)), with the computed spectra scaled by a factor of 0.98. Peak positions in the IRMPD spectra are provided in Table 3, along with unscaled frequencies for each of the $M(NO_3)_3^-$ species derived from the DFT calculations (Table 4). In each of the IRMPD spectra, three prominent absorptions are observed. The two absorptions that appear in the ranges 1400–1550 cm^{-1} and 1250–1350 cm^{-1} in Fig. 3a–d correspond to the antisymmetric nitrate stretching (ν_3) mode, which is split as a result of interaction with the metal ion. The higher frequency component is attributed to stretching of the terminal, non-coordinating N=O moiety, while the lower frequency component is assigned to the antisymmetric O—N—O stretching of the nitrate ligands [1]. The other major absorption in each spectrum appears in the region of 1000–1050 cm^{-1}, and is assigned to the symmetric nitrate stretch, ν_1. The spectral features of the $[M(NO_3)_3]^-$ species measured in this study are consistent with those reported in earlier MIS studies of metal-nitrate species [1–8] as well as our previous IRMPD investigation of $[UO_2(NO_3)_3]^-$ and $Eu(NO_3)_4]^-$ [22].

Table 4
Theoretical vibrational frequencies (cm^{-1}, unscaled) for $[M(NO_3)_3]^-$ derived from DFT calculations

	N=O (ν_3)	O—N—O (ν_3)	$\Delta\nu_3$	Sym. NO_3 (ν_1)
NO_3^-		1377.76, 1377.83	n.a.	1065.74
$[Mg(NO_3)_3]^-$	1558.95, 1559.02	1292.80, 1327.97	230.98	1050.52, 1050.63
$[Ca(NO_3)_3]^-$	1538.22, 1538.32	1286.44, 1308.75	229.47	1051.02, 1051.09
$[Sr(NO_3)_3]^-$	1526.95, 1526.99	1309.02	217.93	1053.33, 1053.36
$[Ba(NO_3)_3]^-$	1515.02, 1515.04	1306.7	208.32	1055.31, 1055.33

The experimental IRMPD spectra are in good general agreement with those predicted using B3LYP/6-311 + g(2d,p)/6-311 + g(d,p) or B3LYP/SDD/6-311 + g(d,p). Table 4 shows that the DFT calculations predict two nearly degenerate bands for the high-frequency component of the ν_3 absorption, regardless of the precursor ion, which are not resolved in the IRMPD spectrum. The two closely spaced absorptions correspond to modes that involve the N = O units of two of the three nitrate ligands.

For $Mg(NO_3)_3^-$, the DFT calculations predict further splitting of the low-frequency component of the ν_3 stretch into two peaks, spaced by 35 cm^{-1}. The splitting is due to the symmetric and antisymmetric combinations of the O—N—O stretches for the three nitrate ligands. A similar splitting of the low-frequency component of ν_3 is also predicted for the Ca complex, although the spacing between the two absorptions is smaller (23 cm^{-1}). The resolution of the IRMPD experiment was not sufficient to resolve the two components, although in the IRMPD spectrum of $Mg(NO_3)_3^-$, the band near 1300 cm^{-1} is significantly broader than the analogous peaks for the other anionic metal-nitrate complexes, which likely indicates the presence of two bands, split by a larger spacing of about 35 cm^{-1}.

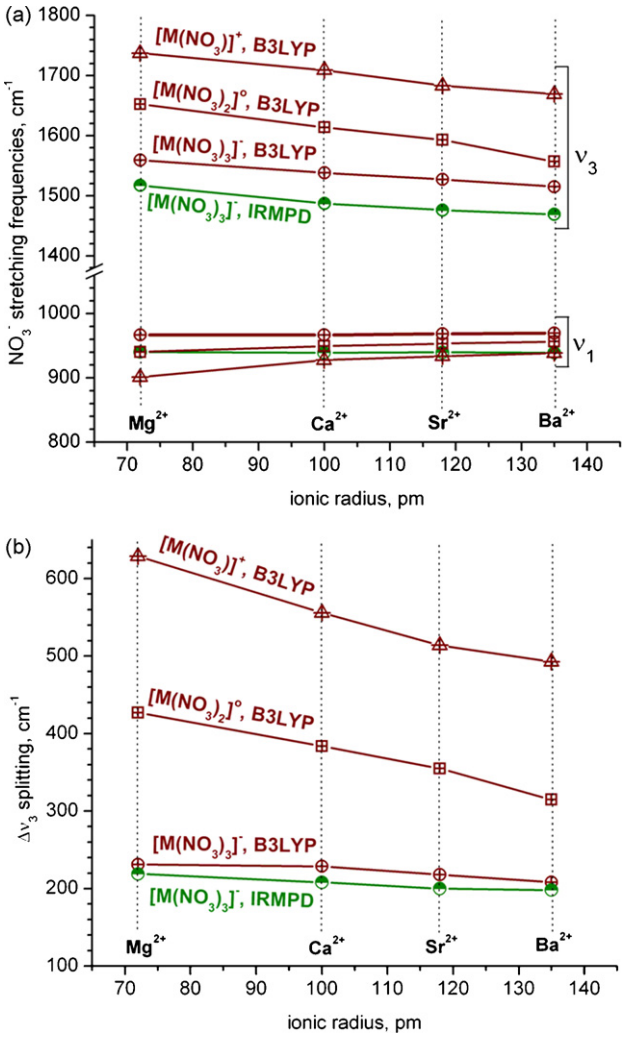

Fig. 7. (a) NO_3^- stretching frequencies plotted versus ionic radius of the coordinated metal cations. The high-frequency ν_3 band and ν_1 bands are plotted. (b) $\Delta\nu_3$ splitting values plotted versus ionic radius. B3LYP calculated values are plotted in red for $M(NO_3)_3^-$ (circles), $M(NO_3)_2^\circ$ (squares), and $M(NO_3)^+$ (triangles). IRMPD values for $M(NO_3)_3^-$ complexes are plotted using green circles.

3.3. Influence of metal ion on splitting of ν_3 stretch

In the respective IRMPD spectra of the $M(NO_3)_3^-$ anions, the position of the high-frequency component of ν_3 shifts to the red with increasing metal ion radius [35] (Fig. 7a). The magnitude of the shift was 48 cm^{-1} as the cation was varied from Mg^{2+} to Ba^{2+}. This trend is accurately predicted by the B3LYP calculations (shift magnitude of 44 cm^{-1}), although the calculated values for the high-frequency ν_3 component were 42–52 cm^{-1} higher than the measurements. A similar trend in the high-frequency component of the ν_3 stretch were calculated for the neutral dintrato complexes, as the cation was changed from Mg^{2+} to Ba^{2+}. The high-frequency ν_3 values were greater, as was the magnitude of the red shift on going from Mg^{2+} to Ba^{2+} (95 cm^{-1}, compared to 44 cm^{-1} for the trinitrato complexes). Calculations of the cationic mononitrato complexes also produced the same trend, with a red shift of 68 cm^{-1} seen when the cation was changed from Mg^{2+} to Ba^{2+}. In contrast to the high-frequency ν_3 component, the positions of the low-frequency ν_3 component less sensitive to cation substitution. In the IRMPD data, a red shift of 27 cm^{-1} was noted as the cation was varied from Mg^{2+} to Ba^{2+}; a similar trend was observed in the B3LYP values, but direct comparison was less straightforward because of the presence of multiple modes for the Mg^{2+} and Ca^{2+} complexes. The symmetric ν_1 band was effectively insensitive to the metal ion.

Table 5
Theoretical vibrational frequencies (cm^{-1}, unscaled) for $[M(NO_3)_2]$ derived from DFT calculations

	N=O (ν_3)	O—N—O (ν_3)	$\Delta\nu_3$	Sym. NO_3 (ν_1)
$[Mg(NO_3)_2]$	1652.07	1225.55, 1225.60	426.52	1010.73
$[Ca(NO_3)_2]$	1613.80	1230.11, 1230.12	383.69	1024.89
$[Sr(NO_3)_2]$	1593.05	1237.75, 1237.76	355.30	1030.33
$[Ba(NO_3)_2]$	1557.44	1241.91, 1241.92	315.53	1034.61

As noted earlier, previous studies of isolated MNO_3 and related species, the magnitude of the *splitting* of the ν_3 absorption ($\Delta\nu_3$) is proportional to the strength of the interaction between the metal ion and the nitrate ligand [1]. Theoretical $\Delta\nu_3$ values for the $M(NO_3)_3^-$ ions investigated in this study as derived from the DFT calculations are listed in Table 4. For the Mg^{2+} and Ca^{2+} complexes, the $\Delta\nu_3$ value given by the average of the two calculated low-frequency ν_3 components is reported.

The DFT calculations predict a general decrease of $\Delta\nu_3$ with increasing ionic radius, with values of approximately 231, 229, 218 and 208 cm^{-1} for Mg^{2+}, Ca^{2+}, Sr^{2+} and Ba^{2+}, respectively (Table 4, Fig. 7b). The experimentally determined $\Delta\nu_3$ values are 219, 208, 200 and 198 for Mg^{2+}, Ca^{2+}, Sr^{2+} and Ba^{2+}, respectively, which qualitatively follow the trend predicted by DFT, although the values are consistently lower than the computed values by anywhere from 10 to 21 cm^{-1}. The $\Delta\nu_3$ values decrease as the cation is changed from Mg^{2+} to Ba^{2+}, following the same qualitative trend observed in the high-frequency ν_3 values. Close examination of plots of ν_3 and $\Delta\nu_3$ versus cation ionic radii showed that the trends were neither linear nor exponential, suggesting that these parameters could not be related by a simple arithmetic relationship.

The $\Delta\nu_3$ values measured for the trinitrato-group II cation complexes provided an opportunity for comparison with prior values acquired for other complexes. Overall, the measured $\Delta\nu_3$ values for the $M(NO_3)_3^-$ anions are lower than those measured by the same technique for $UO_2(NO_3)_3^-$ and $Eu(NO_3)_4^-$ (264 and 274 cm^{-1}, respectively [22]) and lie between those measured for matrix isolated $LiNO_3$ and KNO_3 monomers ($\Delta\nu_3$ of 260 and 171 cm^{-1}, respectively). The most appropriate comparison to make is between the trinitrato species $M(NO_3)_3^-$ investigated in the present study, and the value for $UO_2(NO_3)_3^-$, which shows that the group II metals interact less strongly (based on the magnitude of $\Delta\nu_3$) with nitrate than does the uranyl ion.

As noted above, the alteration in $\Delta\nu_3$ for $M(NO_3)_3^-$ as the cation is changed from Mg^{2+} to Ba^{2+} is modest (based on the IRMPD data and B3LYP calculations), which reflects the fact that the presence of three nitrate ligands in the complexes reduces the extent of perturbation by the metal ion on each of the nitrate ligands. To gain a better understanding of how the number of nitrate ligands influences the magnitude of $\Delta\nu_3$, the values for $M(NO_3)_3^-$ can be compared to those predicted for $M(NO_3)_2$ and $M(NO_3)^+$ by DFT (B3LYP/6-311 + g(2d,p)/6-311 + g(d,p) or B3LYP/SDD/6-311 + g(d,p)) calculations. The vibrational frequencies, including $\Delta\nu_3$ values, predicted for $M(NO_3)_2$ and $M(NO_3)^+$ are provided in Tables 5 and 6, respectively, and are depicted graphically in Fig. 7b. The optimized

Table 6
Theoretical vibrational frequencies (cm^{-1}, unscaled) for $[M(NO_3)]^+$ derived from DFT calculations

	N=O (n_3)	O—N—O (n_3)	Δn_3	Sym. NO_3 (ν_1)
$[Mg(NO_3)_2]$	1737.10	1108.11	628.99	952.49
$[Ca(NO_3)_2]$	1709.03	1153.02	556.01	992.30
$[Sr(NO_3)_2]$	1683.23	1169.49	513.74	1001.23
$[Ba(NO_3)_2]$	1668.77	1175.67	493.10	1008.52

geometries for the species, as well as predicted bond lengths and angles, are provided in the Supporting information. For the neutral $M(NO_3)_2$ species, the $\Delta\nu_3$ values decrease with increasing cation radius and decreasing polarizing power, as observed for the $M(NO_3)_3^-$ anions. However, compared to the trinitrato anions, the predicted alteration in $\Delta\nu_3$ values caused by changing the cation were much larger, varying by approximately 100 cm^{-1}. The $\Delta\nu_3$ ranged from 427 cm^{-1} for $Mg(NO_3)_2$ to 316 cm^{-1} for $Ba(NO_3)_2$.

The trend toward larger $\Delta\nu_3$ values in complexes containing fewer nitrate ligands is further substantiated by calculations for the cationic mononitrato $M(NO_3)^+$ complexes. As in the neutral and anionic complexes, the trend in the $\Delta\nu_3$ values are predicted to decrease with increasing cation radius and decreasing polarizing power for the $M(NO_3)^+$ species. However, the magnitude of the $\Delta\nu_3$ values calculated for the mononitrato cations $M(NO_3)^+$ were on the order of 100 cm^{-1} higher than for the analogous dinitrato neutrals (Fig. 7b), and around 200 cm^{-1} higher than those for the trinitrato anions $M(NO_3)_3^-$. The $\Delta\nu_3$ values ranged from 629 cm^{-1} for $Mg(NO_3)^+$ to 493 cm^{-1} for $Ba(NO_3)^+$.

The comparison of calculated values for the tri-, di- and mononitrato complexes with the respective metal ions suggests that the number of nitrate ligands significantly influence the magnitude of the splitting of ν_3. Even so, the IRMPD data for the trinitrato complexes show that the strength of interaction between metal ion and nitrate ligands, on average, decreases with increasing ionic radius.

4. Conclusions

Infrared multiple-photon dissociation spectroscopy has been applied to record infrared spectra of discrete gas-phase $[M(NO_3)_3]^-$ anions, where M is Mg^{2+}, Ca^{2+}. Sr^{2+} or Ba^{2+}. For each precursor anion, the photodissociation pathway activated by absorption of IR photons was elimination of a neutral $M(NO_3)_2$ unit to yield an NO_3^- anion. Characteristic metal-nitrate ligand bands are observed in the IR spectra of the respective complexes that are in good agreement with those predicted by DFT calculations. The antisymmetric nitrate stretch is split into high- and low-frequency components, consistent with earlier matrix isolation studies of metal-nitrate monomers, and an earlier IRMPD study of $[UO_2(NO_3)_3]^-$ and $[Eu(NO_3)_4]^-$. The magnitude of the splitting, $\Delta\nu_3$, depends on the metal center, decreasing for $Mg^{2+} > Ca^{2+} > Sr^{2+} \cong Ba^{2+}$. The trend observed is consistent with the fact that the $\Delta\nu_3$ value is used to measure the strength of metal ion binding to nitrate. Overall, $\Delta\nu_3$ values measured for the $[M(NO_3)_3]^-$ anions are lower than the values measured for $[UO_2(NO_3)_3]^-$ and $[Eu(NO_3)_4]^-$, which shows that the group II cations interact less strongly with nitrate than does the either the uranyl ion or the Eu(III) cation.

Acknowledgements

Work by M. Van Stipdonk, L. Myers, R. Dain, C. Leavitt and V. Pham is supported in part through a grant from the US National Science Foundation (NSF grant CAREER-0239800) and the Fairmount College of Liberal Arts and Sciences of Wichita State University. Density functional theory calculations were performed at Wichita State University using resources of the High-performance Computing Center (HIPECC), a facility supported by the NSF under Grants EIA-0216178 and EPS-0236913 and matching support from the State of Kansas and HIPECC. Work by G. Groenewold and G. Gresham is supported by the US Department of Energy, Assistant Secretary for Environmental Management, and the INL Laboratory Directed Research & Development Program under DOE Idaho Operations Office Contract DE AC07 05ID14517. J. Oomens is supported by the Nederlandse Organisatie voor Wetenschappelijk Onderzoek (NWO). Construction and shipping of the FT-ICR-MS instrument was made possible through funding from the National High Field FT-ICR Facility (grant CHE-9909502) at the National High Magnetic Field Laboratory, Tallahassee, FL.

Appendix A. Supplementary data

Supplementary data associated with this article can be found, in the online version, at doi:10.1016/j.ijms.2008.02.013.

References

[1] D. Smith, D.W. James, J.P. Devlin, J. Chem. Phys. 54 (10) (1971) 4437.
[2] G. Ritzhaupt, J.P. Devlin, J. Phys. Chem. 61 (1997) 521.
[3] W.A. Guillory, M.L. Bernstein, J. Chem. Phys. 62 (1975) 1058.
[4] G. Ritzhaupt, J.P. Devlin, J. Phys. Chem. 95 (1991) 90.
[5] R.T. Tisdale, A.J. Prenni, L.T. Iraci, M.A. Tolbert, Geophys. Res. Lett. 26 (1999) 707.
[6] N. Barton, B. Rowland, J.P. Devlin, J. Phys. Chem. 97 (1993) 5848.
[7] M.A. Tolbert, A.M. Middlebrook, J. Geophys. Res. 22 (1990) 22.
[8] B.G. Koehler, A.M. Middlebrook, M.A. Tolbert, J. Geophys. Res. 97 (1992) 8065.
[9] J. Oomens, B.G. Sartakov, G. Meijer, G. von Helden, Int. J. Mass Spectrom. 254 (2006) 1.
[10] D.T. Moore, J. Oomens, J.R. Eyler, G. Meijer, G. von Helden, D.P. Ridge, J. Am. Chem. Soc. 126 (2004) 14726.
[11] J. Oomens, D.T. Moore, G. von Helden, G. Meijer, R.C. Dunbar, J. Am. Chem. Soc. 126 (2004) 724.
[12] D.T. Moore, J. Oomens, J.R. Eyler, G. von Helden, G. Meijer, R.C. Dunbar, J. Am. Chem. Soc. 127 (2005) 7243.
[13] A. Fielicke, G. von Helden, G. Meijer, D.B. Pedersen, B. Simard, D.M. Rayner, J. Phys. Chem. B 108 (2004) 14591.
[14] B.M. Reinhard, A. Lagutschenkov, J. Lemaire, P. Maitre, P. Boissel, G. Neidner-Schatteburg, J. Phys. Chem. A 108 (2004) 3350.
[15] T.D. Jaeger, D. van Heijnsbergen, S.J. Klippenstein, G. von Helden, G. Meijer, M.A. Duncan, J. Am. Chem. Soc. 126 (2004) 10981.
[16] D. van Heijnsbergen, G. von Helden, G. Meijer, P. Maitre, M.A. Duncan, J. Am. Chem. Soc. 124 (2002) 1562.
[17] N.C. Polfer, J. Oomens, R.C. Dunbar, Phys. Chem.-Chem. Phys. 8 (2006) 2744.
[18] G.S. Groenewold, A.K. Gianotto, K.C. Cossel, M.J. Van Stipdonk, D.T. Moore, N. Polfer, J. Oomens, W.A. de Jong, L. Visscher, J. Am. Chem. Soc. 128 (2006) 4802.
[19] M.A. Duncan, Ann. Rev. Phys. Chem. 48 (1997) 69.
[20] M.A. Duncan, Int. Rev. Phys. Chem. 22 (2003) 407.
[21] J. Lemaire, M. Boissel, G. Heninger, G. Mauclaire, G. Bellec, H. Mestdagh, A. Simon, S. Le Caer, J.M. Ortega, F. Glotin, P. Maitre, Phys. Rev. Lett. 89 (2002) 273002.
[22] G.S. Groenewold, J. Oomens, W.A. de Jong, G.L. Gresham, M.E. McIlwain, M.J. Van Stipdonk, Phys. Chem. -Chem. Phys. 10 (2008) 1192–1202.
[23] N.C. Polfer, J. Oomens, D.T. Moore, G. von Helden, G. Meijer, R.C. Dunbar, J. Am. Chem. Soc. 128 (2006) 905.
[24] A.G. Marshall, T.-C.L. Wang, T.L. Ricca, J. Am. Chem. Soc. 107 (1985) 7893.
[25] V.N. Bagratashvili, V.S. Letokov, A.A. Makarov, E.A. Ryabov, Multiple Photon Infrared Laser Photophysics and Photochemistry, Harwood, Chur, Switzerland, 1985.
[26] J. Oomens, G.G.M. Tielens, B.G. Sartakov, G. von Helden, G. Meijer, Astrophys. J. 591 (2003) 968.
[27] A.G. Marshall, C.L. Hendrickson, G.S. Jackson, Mass Spectrom. Rev. 17 (1998) 1.
[28] M.J. Frisch, G.W. Trucks, H.B. Schlegel, G.E. Scuseria, M.A. Robb, J.R. Cheeseman, J.A. Montgomery, Jr., T. Vreven, K.N. Kudin, J.C. Burant, J.M. Millam, S.S. Iyengar, J. Tomasi, V. Barone, B. Mennucci, M. Cossi, G. Scalmani, N. Rega, G.A. Petersson, H. Nakatsuji, M. Hada, M. Ehara, K. Toyota, R. Fukuda, J. Hasegawa, M. Ishida, T. Nakajima, Y. Honda, O. Kitao, H. Nakai, M. Klene, X. Li, J.E. Knox, H.P. Hratchian, J.B. Cross, V. Bakken, C. Adamo, J. Jaramillo, R. Gomperts, R.E. Stratmann, O. Yazyev, A.J. Austin, R. Cammi, C. Pomelli, J.W. Ochterski, P.Y. Ayala, K. Morokuma, G.A. Voth, P. Salvador, J.J. Dannenberg, V.G. Zakrzewski, S. Dapprich, A.D. Daniels, M.C. Strain, O. Farkas, D.K. Malick, A.D. Rabuck, K. Raghavachari, J.B. Foresman, J.V. Ortiz, Q. Cui, A.G. Baboul, S. Clifford, J. Cioslowski, B.B. Stefanov, G. Liu, A. Liashenko, P. Piskorz, I. Komaromi, R.L. Martin, D.J. Fox, T. Keith, M.A. Al-Laham, C.Y. Peng, A. Nanayakkara, M. Challacombe, P.M.W. Gill, B. Johnson, W. Chen, M.W. Wong, C. Gonzalez, J.A. Pople, Gaussian 03, Revision D.01, Gaussian, Inc., Wallingford, CT, 2004.
[29] C.T. Lee, W.T. Yang, R.G. Parr, Phys. Rev. B 37 (1988) 785.
[30] A.D. Becke, J. Chem. Phys. 98 (1993) 5648.
[31] A. Bergner, M. Dolg, W. Kuchle, H. Stoll, G. Preuss, Mol. Phys. 97 (1993) 1431.
[32] M. Dolg, H. Stoll, G. Preuss, R.M. Pitzer, J. Phys. Chem. 97 (1993) 5852.
[33] W. Kuchle, M. Dolg, H. Stoll, H. Preuss, Mol. Phys. 74 (1991) 1245.
[34] W. Kuchle, M. Dolg, H. Stoll, H. Preuss, J. Chem. Phys. 100 (1994) 7535.
[35] R.D. Shannon, Acta Cryst. A32 (1976) 751–767.